(4)

PENNSTATE

Applied Research Laboratory

LARGE FLAT PLATE TURBULENT BOUNDARY LAYER EVALUATION

H.L. Petrie
A.A. Fontaine
S.T. Sommer
T.A. Brungart

Technical Memorandum
File No. 89-207
18 May 1990

Copy No. 6

Approved for Public Release. Distribution Unlimited.

Applied Research Laboratory
P.O. Box 30
State College, PA 16804
(814) 865-3031

LARGE FLAT PLATE TURBULENT BOUNDARY LAYER EVALUATION

H. L. Petrie, A. A. Fontaine, S. T. Sommer, T. A. Brungart

Technical Memorandum
File No. 89-207
18 May 1990

Originally Issued as IM on 2 January 1990

From: H. L. Petrie, A. A. Fontaine, S. T. Sommer, T. A. Brungart

Subject: LARGE FLATE PLATE TURBULENT BOUNDARY LAYER EVALUATION

References: See Page 15

Abstract: The flow characteristics of a 3.1m long by 1.22m span large flat plate mounted in the test section of the ARL Penn State 48-inch diameter water tunnel have been evaluated. The turbulent boundary layer (TBL) over the central 50% of the span of the plate was fully developed, two dimensional and has a near zero streamwise pressure gradient. One component laser Doppler velocimeter (LDV) measurements were made at four freestream velocities and at nine streamwise locations on the plate. Resulting friction velocities on the plate varied from 0.175 to 0.45 m/s, approximately. Reynolds numbers, based on streamwise distance from the boundary layer virtual origin, ranged from 4.5 million to 33.5 million. Momentum thickness Reynolds numbers ranged from 6570 to 39,000. This range of momentum thickness Reynolds number is uniquely large for a laboratory flow.

Table of Contents

	Page
Abstract	1
Table of Contents	2
List of Tables	3
List of Figures	4
Nomenclature	5
Introduction	6
The Large Flat Plate	6
Experimental Procedures and Apparatus	7
Results	10
Summary and Conclusions	14
References	15
Tables	16
Figures	18

List of Tables

Table No.		Page
1	Measured Boundary Layer Parameters	16
2	Comparison of Measured Boundary Layer Parameters with Expected Values	17

List of Figures

Figure No.		Page
1	Large Flat Plate Layout	18
2	Velocimeter Pressure Survey, U_e = 6.7m/s	19
3	Mean Velocity Profiles Scaled with Inner Variables at U_e = 9.3m/s and z = 0.0m	20
4	Mean Velocity Profile Variation with Increasing Re_θ; 48-Inch and 12-Inch Tunnel Results	21
5	Variation of U_e/u^* with Re_θ Including Data from Purtell et al (1981) and 12-Inch and 48-Inch Water Tunnel Flat Plate Data	22
6	Large Flat Plate Skin Friction Coefficient, C_f, Data	23
7	Mean Velocity Profiles Scaled in Outer Variables at U_e = 9.3m/s and z = 0.0m.	24
8	Large Flat Plate Velocity Defect Profiles and Equation (6) and (7)	25
9	The shape factor, $H_{12} = \delta^*/\theta$, for the Large Flat Plate Data Compared with Equation (8)	26
10	Streamwise RMS Fluctuation Levels Scaled in Outer Variables, U_e = 9.3m/s and z = 0.0m	27
11	Streamwise RMS Fluctuation Levels Scaled in Inner Variables, U_e = 9.3m/s and z = 0.0m	28
12	Estimation of the Virtual Origin Location	29
13	Mean Velocity Profiles at z = 0.0, 0.305, and 0.457 with U_e = 9.3m/s and x_o = 0.96m	30
14	Mean Velocity Profiles at z = 0.0, 0.152, and 0.305m with U_e = 9.3m/s and x_o = 2.28m	31
15	Streamwise RMS Fluctuation Levels at z = 0.0, 0.305, and 0.457m with U_e = 9.3m/s and x_o = 0.96m	32
16	Streamwise RMS Fluctuation Levels at z = 0.0, 0.152, and 0.305m with U_e = 9.3m/s and x_o = 2.28m	33

NOMENCLATURE

C_f	-	Skin friction coefficient, $C_f = \tau_w/(1/2\rho U_e^2)$
C_p	-	Static pressure coefficient, equation (1)
H or H_{12}	-	shape parameter, δ^*/θ
Re_{SUB}	-	Reynolds number based on the subscript parameter
U	-	Streamwise component mean velocity
U_e	-	Mean streamwise freestream velocity
u^*	-	Friction velocity, $u^* = (\tau_w/\rho)^{1/2}$
u^+	-	U/u^*
u',v'	-	RMS fluctuation level of streamwise and vertical velocity components
x	-	Distance from leading edge
x_o	-	Distance from virtual origin
y	-	Distance above test surface
y^+	-	$y^+ = yu^*/\nu$
z	-	Distance from plate centerline
δ	-	99% Boundary layer thickness
δ^*	-	Displacement thickness
ν	-	Kinematic fluid viscosity
θ	-	Momentum thickness
Π	-	Wake strength parameter, eq. 2
ρ	-	Fluid density
τ_w	-	Shear stress at wall

INTRODUCTION

This report discusses the results of a 48-inch diameter water tunnel large flat plate evaluation and describes the general configuration of the large flat plate model in detail. The experiments were conducted during two separate tunnel entries. Although there were some changes to the configuration of the plate between these two entries, these were not of a nature to affect the boundary layer flow on the test surface of the plate significantly.

The large flat plate is being used to study the skin friction reduction resulting when a polymer solution is injected through narrow inclined slots in the test surface of the plate into the boundary layer flow. The techniques involved in this study include laser induced fluorescence (LIF) to measure the polymer concentration in the boundary layer and drag balances to measure a locally averaged skin friction. As a result, the plate is fitted with an injection slot for the polymer and removable instrumentation ports in the test surface that allow for laser beam access or drag balance placement as is required by the test program. The performance of these features is not the subject of this report.

THE LARGE FLAT PLATE

The large flat plate model is 3.1m (121.7") long with a 1.22m (48") span and it is 0.07m (2.81") thick. The leading edge of the plate consists of a 6 to 1 elliptic nose section made from hard anodized aluminum. The plate is mounted on the horizontal centerplane of the tunnel test section such that the test surface is one half of the plate thickness above the tunnel centerplane. This centers the plate vertically in the test section windows. The mounting attachments to the tunnel sidewalls are internal to the plate.

The top surface of the plate is the test surface and consists primarily of 3 anodized aluminum sheets that span the central 0.76m of the 1.22m width of the plate, see Figure 1. A 0.23m span section of the test surface, extending along each side wall of the tunnel from the nose section to the tail assembly, consists of two separate aluminum sheets or side panels on each side of the plate. All of these plates comprising the test surface are mounted on spacer ribs that are connected to a large stainless steel plate that is the bottom surface. This bottom plate is mounted on two heavy angle iron rails that are attached directly to the water tunnel walls and run the length of the test plate. These iron rails are unintentionally bowed and slightly high at their midpoints. This bow was cancelled partially by shimming the bottom plate level and flat. However, the test surface side panels rest on top of these rails at the sidewalls and were slightly (2mm) high at the tunnel sidewall near the midlength of the plate. Therefore, those side panels were not perfectly flat and horizontal. Since this deviation from level was not realized until after installation of the plate and was not expected to alter the flow over the plate away from the sidewall, the iron rails were not reworked to eliminate the problem.

Each test surface plate is adjusted via set screws and shim stock to provide, as is possible, a flat surface with smooth joint lines.

The three instrumentation ports in the test surface, see Figure 1, can accept clear acrylic window sections for LIF work or stainless steel plates with drag balance assemblies. The three replaceable sections are located 0.6908m, 1.536m, and 2.436m from the leading edge of the plate. The first two sections are 0.471m long by 0.184m wide and the third section is 0.177m long by 0.182m wide. During the first entry an acrylic window was installed at the first location, x = 0.691m, and the downstream two instrumentation ports were not yet present. During the second entry, all instrumentation ports were present and were fitted with stainless steel plates with miniature drag balance assemblies mounted on them.

A 0.21m long symmetric tapered tail section with a 9.5 degree half angle was adjusted to provide a slight negative angle of attack at the nose. This insures a stable attachment of the stagnation streamline on the upper half of the nose section and provides a zero pressure flow over the plate. The bisecting midplane of the tail can be inclined +/- 15 degrees to horizontal, approximately. The larger positive inclination angles that were tried first could not be maintained due to the forces on the tail. Sidewall attachments were added to support the tail but these restricted the range of inclination of the tail midplane from +5.5 to +15 degrees. A +6.0 degree inclination of the tail was sufficient for a stable flow at the nose, based on the resulting boundary layer data.

Increasing the tail angle shifts the dividing streamline downstream from the nose. The virtual origin was shifted from approximately 0.06m upstream to approximately 0.25m downstream of the plate leading edge for a tail angle variation from 6.0 to 13.0 degrees respectively. This has an effect on the TBL integral thicknesses that diminished with increasing streamwise distance. By x = 2.0m, the effect of such changes in the virtual origin location on the integral thicknesses is only 2%. Larger tail angles also increase the amount of fluid that must move under the plate and therefore increases the pressure differential between the top and bottom of the plate. This loads the plate unnecessarily and causes a measurable deflection of the test surface in the middle of the plate. Therefore, the smaller angle is preferred. A tail angle of 13.0 degrees caused, approximately, a 2mm downward shift of the top surface of the plate near its midpoint when the velocity was increased from 4.6 to 13.7 m/s. A strut will be mounted on the bottom side of the plate in future tests to minimize the downward plate displacement.

The center 0.041m (1.625") of the plate between the top and bottom surfaces is largely empty with the exception of the spacer ribs and can be used for storage and routing of instrumentation and wires. However, during testing this area is wet since there are numerous openings in the sides of the plate and seams on the top and bottom surfaces are not sealed. Adequate water proofing of hardware stored here is necessary.

It was observed that dyed fluid pumped into the injection slot assembly, which should pass through the slot into the fluid layer immediately adjacent to the test surface, was somehow leaking into the interior of the plate. It is believed that at least part of this leakage was through the seams in the test surface of the plate since no substantial leakage was detected in the supply plumbing or slot assembly. This seepage through these seams could be the result of the pressure difference between the top and bottom surface of the plate due to the tail on the plate. The pressure differential induces a flow from the test surface to the bottom surface through any of the available routes such as seams in the plate.

Gaps were present between two side panel sheets at both sides of the plate test surface and, in particular, between the side of the plate and the tunnel sidewalls and windows. The two side panel gaps, approximately 2.5mm (0.1") wide, are the result of poorly fitted pieces. The gaps between the plate and the sides of the tunnel prevented damage to the tunnel windows. The windows are acrylic and would be scratched by the plate if contact were allowed. These gaps and other small openings on the bottom of the plate allow a flow into and through the plate. The flow from the top surface towards the bottom at these sidewall gaps is a suction that can reduce sidewall contamination, see Motohashi and Blackwelder (1983), and there is evidence that this is the case in the data discussed below.

The experiments were performed with an injection slot assembly mounted on the plate 0.64m downstream from the plate leading edge, see Figure 1. A second slot assembly will be added in the near future 1.485m downstream of the leading edge. The convergent internal walls comprising the slot are inclined at a mean angle of 25 degrees with respect to the plate surface and the slot width at the test surface is 2.54mm. The slot spans the center 0.641m of the plate. A small plenum below the slot is baffled to increase the pressure drop across the slot assembly to provide a uniform injection flow over the span of the slot. Three lines enter through the side of the plate through the upstream test section window to supply the slot assembly with polymer and three more lines are available for a second slot.

EXPERIMENTAL PROCEDURES AND APPARATUS

A one component fringe mode laser Doppler velocimeter (LDV) was used to survey the boundary layer on the plate and to evaluate the streamwise and spanwise variation of the freestream velocity above the plate. Doppler signals from the LDV were processed using a counter type processor. One beam of the two beam system was frequency shifted at an effective frequency shift of 2 MHz. The LDV was used in a forward scatter mode for the boundary layer surveys and in a backscatter mode for the freestream velocity surveys. Either a 750mm or a 450mm nominal focal length lens was used for the LDV focussing optics as was required. The forward scatter collection lens focal length was 580mm or 900mm as needed. Resulting data rates ranged from 2000 to 12,000 validated bursts per second in the forward scatter mode, and approximately 300 to

500 in the backscatter mode. The tunnel was seeded with silicon carbide particles with a mean diameter of 1.5 microns and a specific gravity of 3.2. The LDV determined freestream turbulence levels in the forward scatter mode were less than 0.4% indicating a relatively clean Doppler signal. The bare tunnel turbulence level is less than 0.1%. The backscatter freestream "turbulence" level was typically twice the forward scatter value.

The LDV transmitting optics were inclined approximately 2 degrees with respect to the horizontal plane of the test plate to improve optical access. In the forward scatter mode, LDV transmitting and receiving optics were mounted on separate structurally sturdy bases, each with traversing capabilities. The receiving optics, in the backscatter mode, were mounted on the same base as the transmitting optics and on the optical centerline. The LDV could be traversed in three directions with an uncertainty of +/-0.0127mm. The location of the plate surface was determined by visual inspection of the LDV beam crossover and the filtered Doppler signal output on an oscilloscope as the wall was approached. The wall location could be determined with an uncertainty of +/-0.025mm.

The variation of the freestream velocity above the plate at a constant tunnel condition was evaluated by LDV measurements at locations along the length of the plate. The freestream velocity measurements can be related to the pressure coefficient on the plate by the following relation:

$$C_p = 1 - (U/U_{ref})^2 = \frac{p \quad p_{ref}}{1/2 \ \rho \ U_e^2} \qquad (1)$$

where U_{ref} is the value of the freestream velocity at a reference location above the plate and equals U_e. Often, the pressure coefficient is formulated using the stagnation pressure rather than the reference static pressure in Equation 1. When this is done, $C_p = -(U/U_e)^2$ results. Thus, the difference between these two approaches is an additive constant, 1. These velocimeter "pressure" surveys have the advantage that they can be measured anywhere above the plate but require that the tunnel condition be maintained for the duration of the survey. This is reasonable to assume because the tunnel impeller RPM and blade pitch angle can be maintained accurately during the course of a survey and these "pressure" surveys proceeded relatively rapidly. Surveys were performed at three spanwise positions, z = 0.0m, 0.3048m, and 0.457m from the centerline of the plate. Static pressure taps were located on a line 0.483m off of the tunnel centerline. However, these static taps were too close to the sidewall to be free of its influence and too far from the centerline to be generally useful.

Boundary layer surveys were measured at nine streamwise and four spanwise positions. The positions are shown in Figure 1 and listed in the table insert of Figure 1. LDV boundary layer and freestream

velocity surveys were conducted at four freestream velocities, approximately 4.5, 6.7, 9.3 and 13.7 m/s. In both the freestream velocity surveys and the boundary layer surveys, the effect of varying the tail angle was investigated. Three tail angles, with the tail midplane bisector inclined 13.0, 9.5, and 6.0 degrees above horizontal, were studied.

Velocimeter pressure surveys and boundary layer profiles were also measured with and without a tunnel liner in the first tunnel entry. A liner had been designed and built to ensure a zero axial pressure gradient flow on the plate. The desired effect of the liner was to offset the accelerating nozzle effect of the growing boundary layers on the plate and tunnel walls. The liner consisted of two separate pieces to modify the flow on both the top and bottom sides of the plate in a similar fashion. The data show that the liners have no substantial effect. Both liners were removed after the skin on one started to break free in one section and the liners have not been used since. The large amount of time to install the liners and the resultant loss of optical access to the top of the plate from the tunnel hatch windows were other reasons for not using the liners.

LDV data acquisition and reduction were performed on a PC/AT computer. The friction velocity, u^*, and pressure gradient parameter, Π were determined by a least squared error fit of the boundary layer velocity data to the law of the wall plus Coles wake function, equation (2), see Deutsch and Zierke (1986).

$$u^+ = (1/0.41)\ \ln(y^+) + 5 + (\Pi/0.41)[1 - \cos(\frac{\pi y}{\delta})] \qquad (2)$$

A graphical Clauser plot routine was also used as a check for the estimated friction velocity. The estimated uncertainties, to the 95% confidence level, in the evaluated u^* and Π values are +/-6% and +/-10% respectively. Integral thicknesses were estimated by three methods. Numerical integration of the profile data using a trapezoidal rule, numerical integration of a spline curve fit to the profile data, and numerical integration of equation (2) with the estimated values of u^* and Π. Very good agreement was obtained between the three methods.

RESULTS

The streamwise pressure gradients were inferred from the freestream velocity surveys measured above the plate along its length. The velocimeter "pressure" surveys indicated a zero pressure gradient flow exists over the plate. Typical velocimeter C_p results are shown in Figure 2, for a freestream velocity of U_e = 6.7m/s and three spanwise positions. A pressure anomaly exists at the downstream end of the first instrumentation port on the centerline. This may be due to a slight wave in the acrylic window that was in place during these surveys, or from the window not being perfectly flush with the plate. The C_p profile at z = 0.457m shows probable effects of the tunnel sidewall

contamination and/or suction and the freestream velocity values are 1.5% lower than over the rest of the plate as a result of these viscous effects. The observed C_p variation in the data at z = 0 and 0.3048m would result from the freestream velocity variations less than +/-0.5% and is probably, in part, due to the uncertainty in the freestream velocity measurements, +/-0.3%

Mean velocity profile measurements indicate that the TBL flow is fully developed and two dimensional with a zero pressure gradient over the center 0.610m span of the plate. Typical mean velocity profiles measured along the plate centerline are shown in Figure 3 at a nominal freestream velocity of U_e = 9.3m/s; these are plotted in wall variables $u^+ = u/u^*$ and $y^+ = yu^*/\nu$. Equation (2) represents the data well for $y^+>100$. The curve of equation (2), fit to various data with $u^+ = y^+$ used in the viscous sublayer, is plotted in Figure 4 to show the trends in flat plate TBL velocity profile data over a wider range of Reynolds number. Results from an ARL/Penn State 12-inch water tunnel flat plate test with U_e = 4.6m/s and Re_θ = 3090 are included for comparison.

It can be seen in these two figures that there is a continuous growth of the log region and displacement of the wake region of the boundary layer to larger u^+ and y^+ values. U_e/u^* increases with Reynolds number, and the trend in U_e/u^* versus Re_θ is shown in Figure 5 with data from Purtell et al (1981) and our own 12-inch water tunnel data included for comparison. Since:

$$(U_e/u^*) = (2/C_f)^{1/2}, \qquad (3)$$

C_f values exhibit an opposite trend. The C_f results, determined from the mean profiles, are shown in Figure 6 versus Re_{x_o} and are compared with the relationship:

$$C_f = 0.455/\ln^2(0.06\ Re_{x_o}) \qquad (4)$$

Equation (4) is a curve fit simplification of the implicit formulation by Kestin and Persen (1962) and is claimed to be +/-2% accurate, see White (1974). Table 2 also includes a comparison of C_f data with a simpler power law formula.

In terms of wall units, y^+, the log region is increasing in thickness with increasing Reynolds number on Figures 3 and 4. As a fraction of the 99% boundary layer thickness, however, the log layer appears to decrease in size at the highest Reynolds number. These trends were observed at lower Reynolds number by Purtell, et al (1981).

Figure 7 displays the mean velocity profiles of Figure 3 scaled in outer variables. At each freestream velocity, the mean velocity

profiles measured along the plate collapsed reasonably well away from the wall but the profiles exhibit a slightly fuller form below $y/\delta = 0.2$ with increasing Re_x. Hinze (1975) mentions that experiments indicate the 1/n exponent in the power law formula for the mean velocity profile of the form:

$$U/U_e = (y/\delta)^{1/n} \tag{5}$$

is Reynolds number dependent with n increasing with Reynolds number. This results in fuller profiles with increasing Re_x as observed.

The mean velocity profile data in the outer flow should collapse reasonably well if plotted as a velocity defect, $(U-U_e)/u^*$, versus distance from the wall in outer variables. This is done in Figure 8 for various large flat plate data. A curve for the log region in these variables obtained by Clauser (1956) is:

$$(U_e - U)/u^* = -2.44\ln(y/\delta) + 2.5 \tag{6}$$

and is valid for $y/\delta < 0.15$, approximately. The location where deviation from this relationship begins with increasing distance from the wall is Reynolds number dependent, Clauser (1956). A curve fit by Hama (1954):

$$(U_e - U)/u^* = 9.6(1-y/\delta)^2 \tag{7}$$

is shown for the outer part of the boundary layer in Figure 8.

The shape factor, H_{12}, is given by the relationship:

$$H_{12} = [1 - G/(2/C_f)^{1/2}]^{-1},$$

where G is an integral parameter involving Clauser's defect thickness, see White (1974). An approximate value for G based on a curve fit by Nash (1965) for pressure gradient effects is $G = 6.51$ with zero pressure gradient. Using this value for G and equation (3), the relationship for H_{12} may be expressed as:

$$H_{12} = [1 - 6.51u^*/U_e]^{-1}. \tag{8}$$

Hama (1954) found that a relationship of the same form as equation (8) followed his data well but the value of the constant is 6.1 rather than

6.51. Hinze (1975) suggests that Hama's value for the constant is low. The data are compared with equation (8) in Figure 9. The dashed curves on Figure 9 are 3% above and below equation (8) and most of the 48-inch tunnel data falls between these two curves.

The streamwise turbulent rms velocity fluctuation profiles, scaled with outer variables, is shown in Figure 10 with data from Klebanoff (1955). Good agreement was obtained between the LDV profile data at all freestream velocities and the two dimensional zero pressure gradient TBL results of Klebanoff. The excellent collapse of the profiles indicates a fully developed TBL according to Klebanoff. Figure 11 shows these same data scaled in inner variables with comparison to lower Reynolds number data from Purtell et al (1981). The fact that these data do not collapse with inner scaling is used by Wei and Wilmarth (1989) to argue that the turbulence near the wall is still evolving or changing with increasing Reynolds number towards a limit at a high Reynolds number. However, their key concerns involved the lack of inner scaling of Reynolds stress and v' data, especially for $y^+ < 100$. Wei and Wilmarth (1989) postulate that the inner region vorticity field is stretched to a degree greater than that dictated by inner scaling laws as the Reynolds number increases. The displacement or stretching of the u' data trends in Figure 11 away from the wall with increasing Re_θ corresponds closely with the log region growth shown in Figure 4.

Table 1 lists the boundary layer characteristics measured along the centerline on the plate. A comparison of the measured TBL parameters with those computed from standard, high Reynolds number, two dimensional TBL empirical relations, White (1974), is given in Table 2. All streamwise distances are measured from the boundary layer virtual origin, x_o. The excellent agreement obtained between the measurements and the calculated results add further confirmation of a two dimensional zero pressure gradient TBL.

Boundary layer virtual origins were estimated using the evaluated displacement and momentum thicknesses, δ^* and θ. Since for a flat plate TBL both δ^* and θ are proportional to the distance from the virtual origin to the 6/7 power, White, (1974), the virtual origin can be linearly extrapolated from a plot of $\delta^{*7/6}$ and $\theta^{7/6}$ versus streamwise distance from a reference location. A representative plot of the displacement and momentum thicknesses to the 7/6 power versus x, used to estimate the virtual origin, is shown in Figure 12. Typically plots of displacement and momentum thickness data to the 7/6 power versus x show some significant deviation from linearity due to the uncertainties in the integral thickness estimates and relatively short streamwise distances. However due to the large length of the plate, excellent linearity of the integral thickness data to the 7/6 power with streamwise distance was obtained for all measurements.

LDV profile data measured off the centerline show that the three dimensional corner disturbances may be propagating out from the intersection of the tunnel wall with the plate at a smaller angle than 10 degrees, downstream of the x = 0.9m location. Figures 13 and 14 show

spanwise variation of the mean velocity profiles at U_e = 9.3m/s and two streamwise locations, x = 0.9m and 2.53m measured from the plate leading edge. The corresponding rms velocity profiles at the same conditions are shown in Figures 15 and 16. The corner flow effects are apparent in the data at z = 0.457m in Figures 13 and 15, at x = 0.9m, indicating a wedge growth of approximately 10 degrees beginning within 4cm of the nose. However at x = 2.53m, the effects of the three dimensional corner flow are not apparent in the data of Figures 14 and 16, within experimental uncertainty. For a 10 degree wedge growth, the disturbance should have propagated out to z = 0.16m, at x = 2.53m. This indicates that the sidewall wedge growth rate may be smaller than 10 degrees. This could result from the flow into the gap, at the plate to sidewall juncture, inhibiting the growth of the corner flow. Another possibility is that the sidewall effects seen at position 5 on Figure 1 are not due to wedge growth but, say, from the gap between the side panels. If 10° wedge growth does not begin until downstream of x = 0.8m for the 9.3m/s case, then sidewall effects would not be seen at any of the measurement positions. However, this would require sidewall transition not to occur until $Re_{x_o} = 8 \times 10^6 = 1{,}000{,}000$, approximately.

SUMMARY AND CONCLUSIONS

A two dimensional, fully developed, zero pressure gradient TBL flow exists over the center 0.61m span on the top surface of the large flat plate. The plate has been tested over a velocity range of 4.6 to 13.7m/s. Reynolds numbers, based on streamwise distance and momentum thickness, ranged from 4.5 million to 33.5 million and 6570 to 39,000 respectively. The Reynolds number range is uniquely large and begins at the point that the majority of existing data stops.

The tunnel liner did not influence the TBL significantly and thus a liner is not needed or recommended unless specific pressure gradient profiles are desired. For a zero pressure gradient, the liner merely adds to the complexity and time required for the installation and removal of the plate. Variation of the tail angle affected the location of the TBL virtual origin and large tail angles can load the plate excessively. Therefore, a 6.0 degree angle is the maximum recommended. It is advisable that one component boundary layer profiles be measured to check the location of the virtual origin upon installation. This would ensure accurate estimation of boundary layer thicknesses using standard empirical relations at any location on the plate.

Displacement of the plate center, due to the pressure differential between the top and bottom of the plate created by the asymmetric tail, was observed. A strut, mounted to the underside of the plate, will be used to try to resolve this problem in future tests.

There is a significant flow through the plate, and while having no apparent effect on the TBL on the top of the plate other than apparently slowing sidewall contamination, it can affect other types of measurements with instruments mounted in the instrumentation ports provided in the plate. For example, drag balances and LIF work when the

laser beam passes through the plate interior. There is no easy solution to this problem since sealing the plate would not be a trivial task. Future experiments should be aware of this when designing hardware for the flat plate.

REFERENCES

Clauser, F. H., Advances in Applied Mechanics, V4, p. 1, 1956.

Deutsch, S. and Zierke, W. C., "The Measurement of Boundary Lyers on a Compressor Blade in a Cascade at High Positive Incidence Angle," NASA CR-1 4092, August 1986.

Hama, F. R., Soc. Naval Architects Marine Engr. Trans., V62, p. 333, 1954.

Hinze, J. O., Turbulence, McGraw Hill, New York, 2nd Edition, pp. 626-633, 1975.

Kestin, J. and Persen, L. N., Int. J. Heat Mass Transfer, V5, pp. 355-372, 1962.

Klebanoff, P. S., "Characteristics of Turbulence in a Boundary Layer with Zero Pressure Gradient," National Bureau of Standards Report 1247, 1955.

Motohashi, T. and Blackwelder, R. F., "Decreasing Sidewall Contamination in Wind Tunnels," J. of Fluids Engr., ASME, V105, pp. 435-438, December 1983.

Nash, J. F., Natl. Phys. Lab., England, Aero. Report 1137, (see also AGARDograph 97, pp. 245-279), 1965.

Purtell, L. P., Kelbanoff, P. S., and Buckley, F. T., "Turbulent Boundary Layer at Low Reynolds Number," Phys. Fluids, V5, N5, pp. 802-811, May 1981.

Wei, T. and Wilmarth, W. W., "Reynolds-Number Effects on the Structure of a Turbulent Channel Flow," JFM, V204, pp. 57-95, 1989.

White, F. M., Viscous Fluid Flow, McGraw Hill, 1st Edition, pp. 468-483, 1974.

TABLE 1.

	x_o m	U_e m/s	δ_{99} mm	δ^* mm	θ mm	H	$Re_{xo}\ 10^7$	$Re_{\delta^*}\ 10^2$	$Re\theta\ 10^3$	u^* m/s	C_f
+	0.694	6.7	8.89	1.36	0.98	1.39	0.458	9.11	6.57	0.249	0.0028
		9.37	8.78	1.42	0.99	1.43	0.651	13.31	13.31	0.336	0.0026
+	0.77	6.66	10.01	1.50	1.12	1.35	0.514	9.99	7.99	0.248	0.0028
		9.42	10.06	1.55	1.14	1.36	0.722	14.6	10.74	0.336	0.0025
+	0.959	6.71	12.55	1.80	1.36	1.33	0.640	12.08	9.13	0.244	0.0026
		9.4	13.41	1.92	1.44	1.33	0.899	18.05	13.54	0.328	0.0024
+	1.176	6.60	15.44	2.19	1.66	1.32	0.78	14.45	10.96	0.236	0.0026
		9.23	14.97	2.22	1.71	1.30	1.102	20.49	15.78	0.321	0.0024
		4.67	20.9	2.82	2.15	1.31	0.677	13.2	10.0	0.173	0.0027
++	1.45	9.24	20.2	2.56	1.98	1.295	1.34	23.7	18.3	0.326	0.0025
		13.6	18.1	2.3	1.8	1.28	1.97	32.0	24.3	0.47	0.0024
++	1.72	4.47	23.7	3.4	2.5	1.36	0.77	15.3	11.2	0.162	0.0026
		13.35	22.2	2.8	2.1	1.32	2.3	37.7	28.6	0.451	0.0023
		4.42	21.4	3.1	2.38	1.32	0.77	13.8	10.5	0.16	0.0026
+	1.759	6.68	23.03	2.98	2.31	1.29	1.17	19.8	15.4	0.236	0.0025
		9.31	22.1	3.1	2.33	1.33	1.65	28.9	21.7	0.317	0.0023
		13.41	20.7	2.53	1.94	1.304	2.35	31.0	26.0	0.45	0.00225
+	2.029	6.26	26.6	3.43	2.67	1.28	1.27	21.4	16.7	0.221	0.0025
		9.05	27.6	3.25	2.58	1.26	1.83	29.4	23.4	0.311	0.0024
		4.37	29.2	3.9	3.0	1.30	0.92	17.1	13.1	0.156	0.0025
++	2.10	8.92	26.6	3.6	2.7	1.31	1.87	32.0	24.3	0.302	0.0023
		3.7	25.7	3.3	2.6	1.30	2.88	45.5	35.1	0.451	0.0022
++	2.28	4.487	29.5	4.1	3.1	1.31	1.0	18.4	14.0	0.159	0.0025
		8.94	29.2	3.8	2.9	1.29	2.04	33.9	26.2	0.301	0.0023
++	2.43	13.8	28.2	3.6	2.83	1.27	3.35	49.6	39.0	0.456	0.0022

MEASURED BOUNDARY LAYER PARAMETERS

+: virtual origin = -0.06m ++: virtual origin = +0.25m

TABLE 2.

x_o m	U_e m/s	δ_{99} mm	δ_{99} [a] mm	δ^* mm	δ^* [a] mm	θ mm	θ [a] mm	u^* m/s	u^* [c] mm	$C_f 10^{-3}$	C_f [b] 10^{-3}
0.694	6.7	8.89	10.84	1.36	1.4	0.98	1.09	0.249	0.255	2.8	2.9
	9.37	8.78	10.33	1.42	1.33	0.99	1.03	0.336	0.347	2.6	2.76
0.77	6.66	10.01	11.86	1.50	1.53	1.12	1.18	0.248	0.251	2.8	2.86
	9.42	10.06	11.29	1.55	1.45	1.14	1.13	0.336	0.346	2.5	2.72
0.959	6.71	12.55	14.3	1.80	1.84	1.36	1.43	0.244	0.249	2.6	2.77
	9.4	13.41	13.63	1.92	1.75	1.44	1.36	0.328	0.340	2.4	2.64
1.176	6.60	15.44	17.07	2.19	2.19	1.66	1.705	0.236	0.241	2.6	2.7
	9.23	14.97	16.27	2.22	2.09	1.71	1.62	0.321	0.329	2.4	2.57
1.45	4.67	20.9	21.4	2.82	2.75	2.15	2.14	0.173	0.173	2.7	2.75
	9.24	20.2	19.5	2.56	2.5	1.98	1.94	0.326	0.324	2.5	2.5
	13.6	18.1	18.4	2.3	2.4	1.80	1.87	0.47	0.464	2.4	2.4
1.72	4.47	23.7	25.0	3.4	3.2	2.5	2.5	0.162	0.163	2.6	2.7
	13.35	22.2	21.4	2.8	2.75	2.1	2.14	0.451	0.450	2.3	2.3
1.759	4.42	21.4	25.3	3.1	3.25	2.38	2.50	0.16	0.162	2.6	2.7
	6.68	23.03	24.07	2.98	3.1	2.31	2.41	0.236	0.237	2.5	2.54
	9.31	22.1	22.95	3.1	2.95	2.33	2.27	0.317	0.322	2.3	2.42
	13.41	20.7	21.7	2.53	2.8	1.94	2.18	0.45	0.452	2.25	2.3
2.029	6.26	26.6	27.45	3.43	3.53	2.67	2.75	0.221	0.22	2.5	2.51
	9.05	27.6	26.04	3.25	3.35	2.58	2.6	0.311	0.31	2.4	2.38
2.10	4.37	29.2	29.9	3.9	3.8	3.0	2.96	0.156	0.157	2.5	2.6
	8.92	26.6	26.8	3.6	3.4	2.70	2.64	0.302	0.305	2.3	2.4
	3.7	25.7	25.3	3.3	3.25	2.6	2.53	0.451	0.455	2.2	2.2
2.28	4.487	29.5	31.2	4.1	4.0	3.1	3.1	0.159	0.161	2.5	2.6
	8.94	29.2	28.9	3.8	3.7	2.9	2.88	0.301	0.304	2.3	2.35
2.43	13.8	28.2	28.6	3.6	3.7	2.83	2.88	0.456	0.454	2.2	2.2

a: $\delta_{99}, \delta^*, \theta = \dfrac{C\nu\ Re_{xo}^{6/7}}{U_e}$ b: $C_f = 0.026\ Re_{xo}^{-1/7}$ c: $u^* = 0.477\ \dfrac{U_e}{\ln(0.06\ Re_{xo})}$

C = 0.14, 0.018, 0.014

Comparison of Boundary Layer Parameters with Theoretical Values

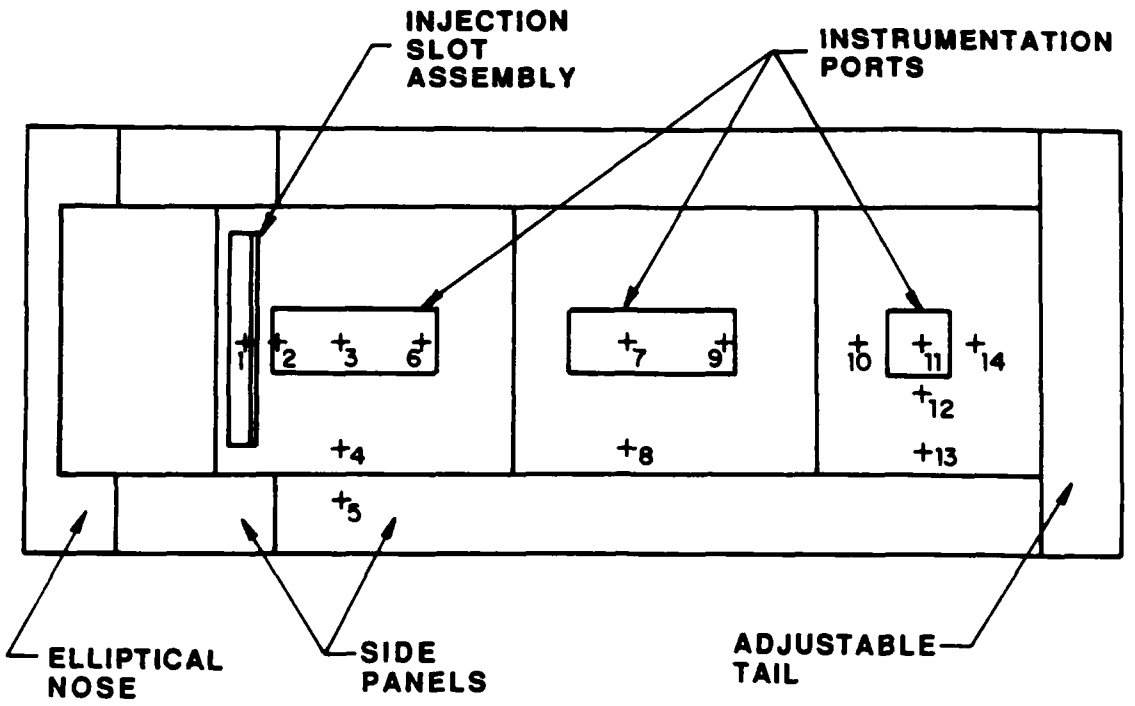

LDV MEASUREMENT LOCATIONS

Position#	x(m)	z(m)
1	0.635	0.0
2	0.711	0.0
3	0.9	0.0
4	0.9	0.305
5	0.9	0.457
6	1.117	0.0
7	1.7	0.0
8	1.7	0.305
9	1.97	0.0
10	2.35	0.0
11	2.53	0.0
12	2.53	0.127
13	2.53	0.305
14	2.68	0.0

Figure 1. Large Flat Plate Layout

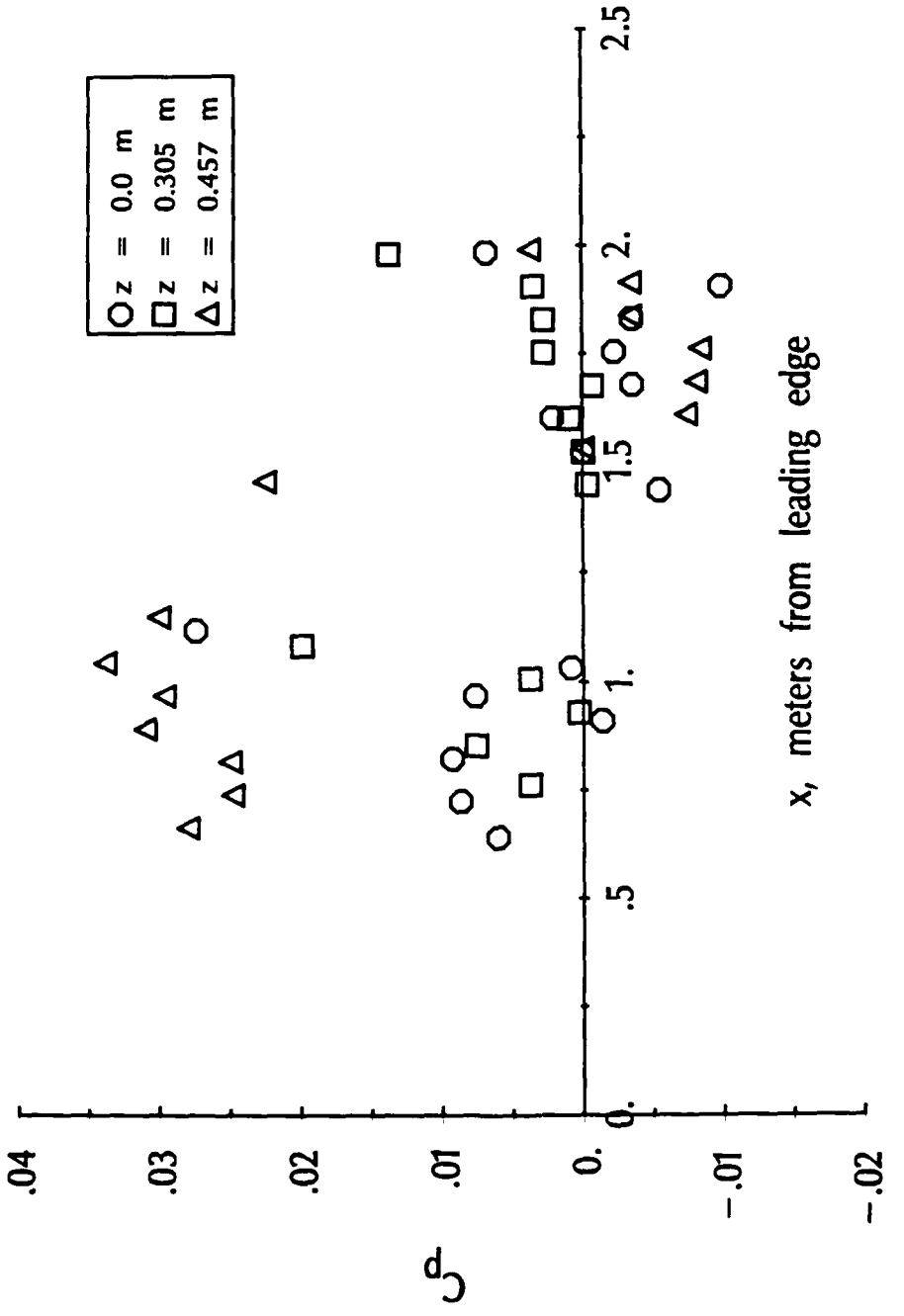

Figure 2. Velocimeter Pressure Survey, U_e = 6.7m/s

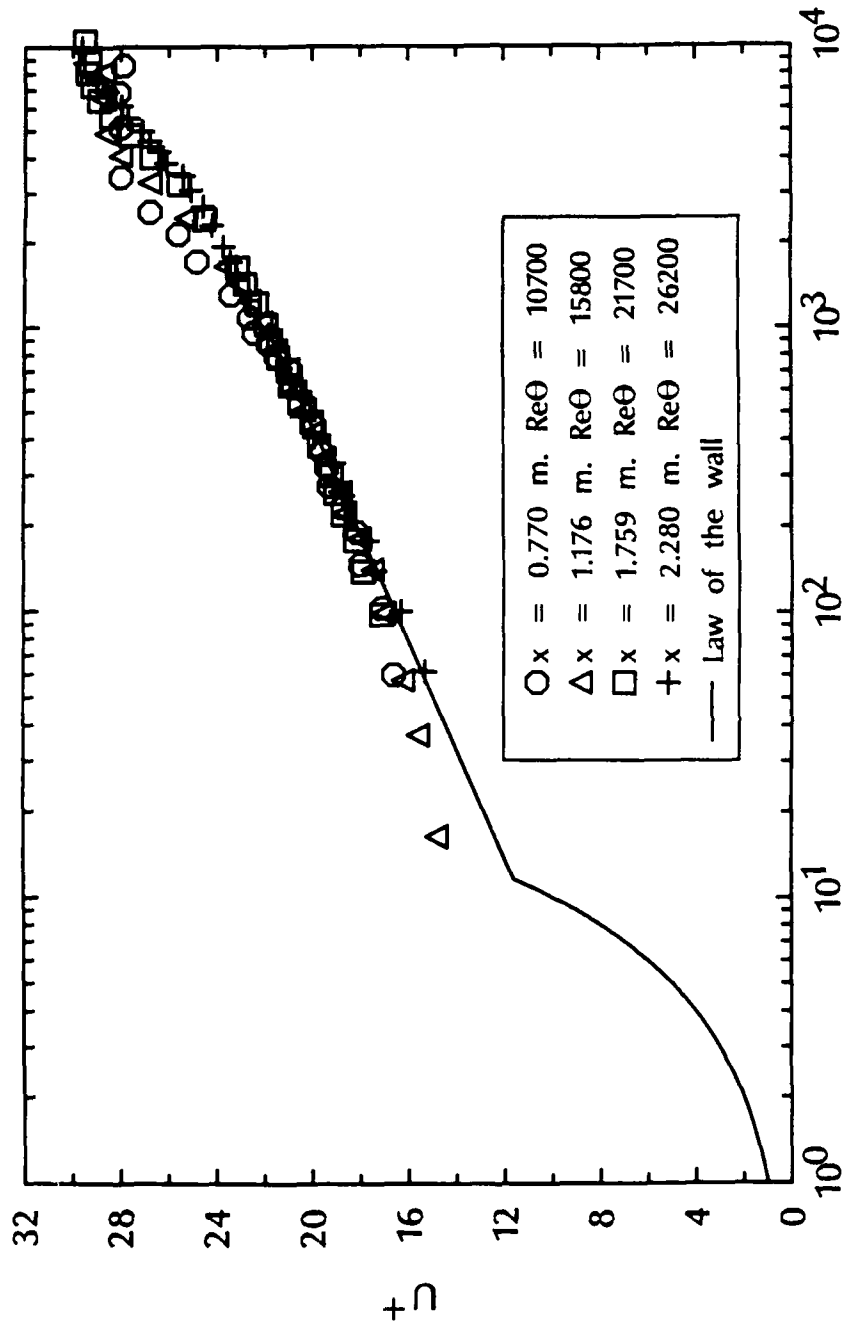

Figure 3. Mean Velocity Profiles Scaled with Inner Variables at U_e = 9.3m/s and z = 0.0m

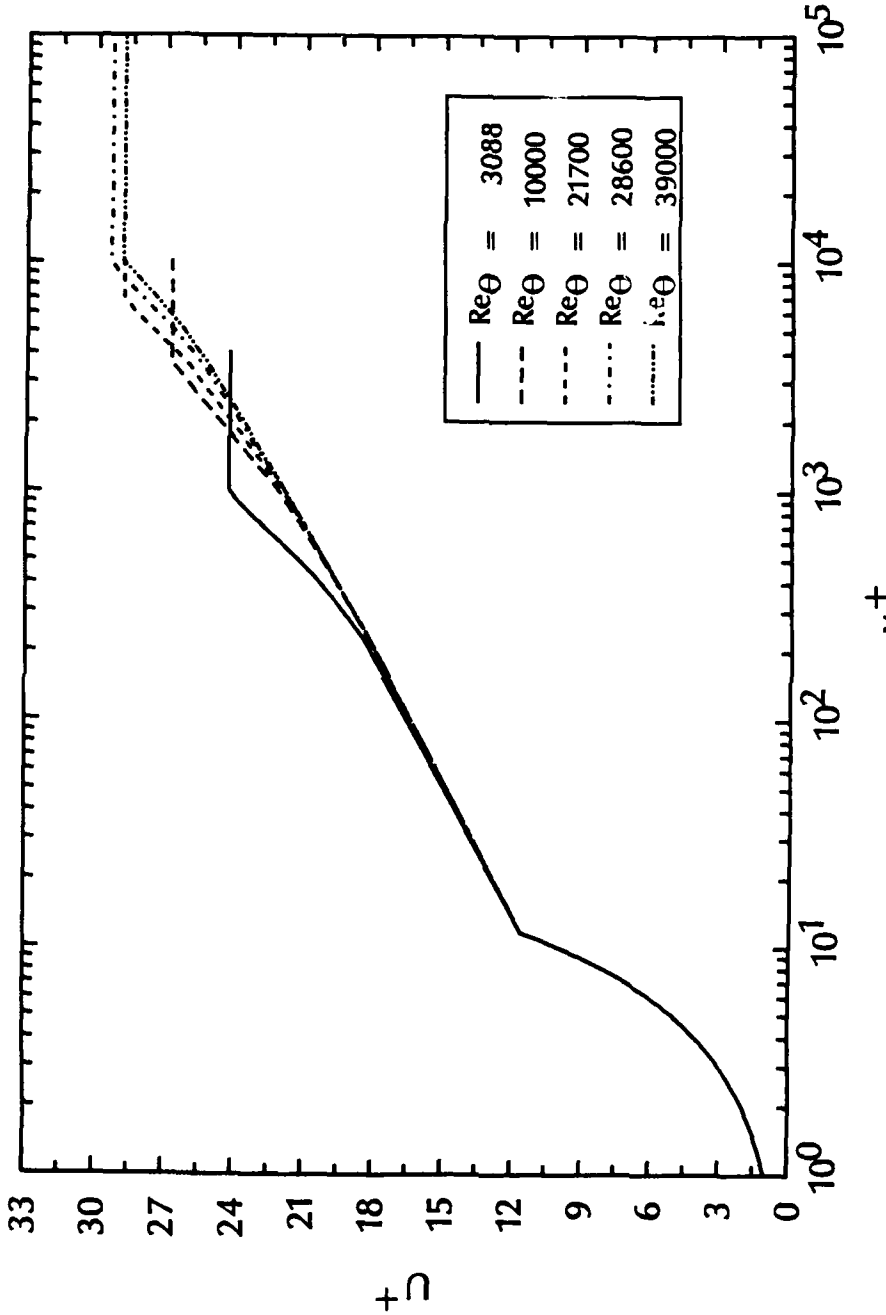

Figure 4. Mean Velocity Profile Variation with Increasing Re_θ; 48-Inch and 12-Inch Tunnel Results

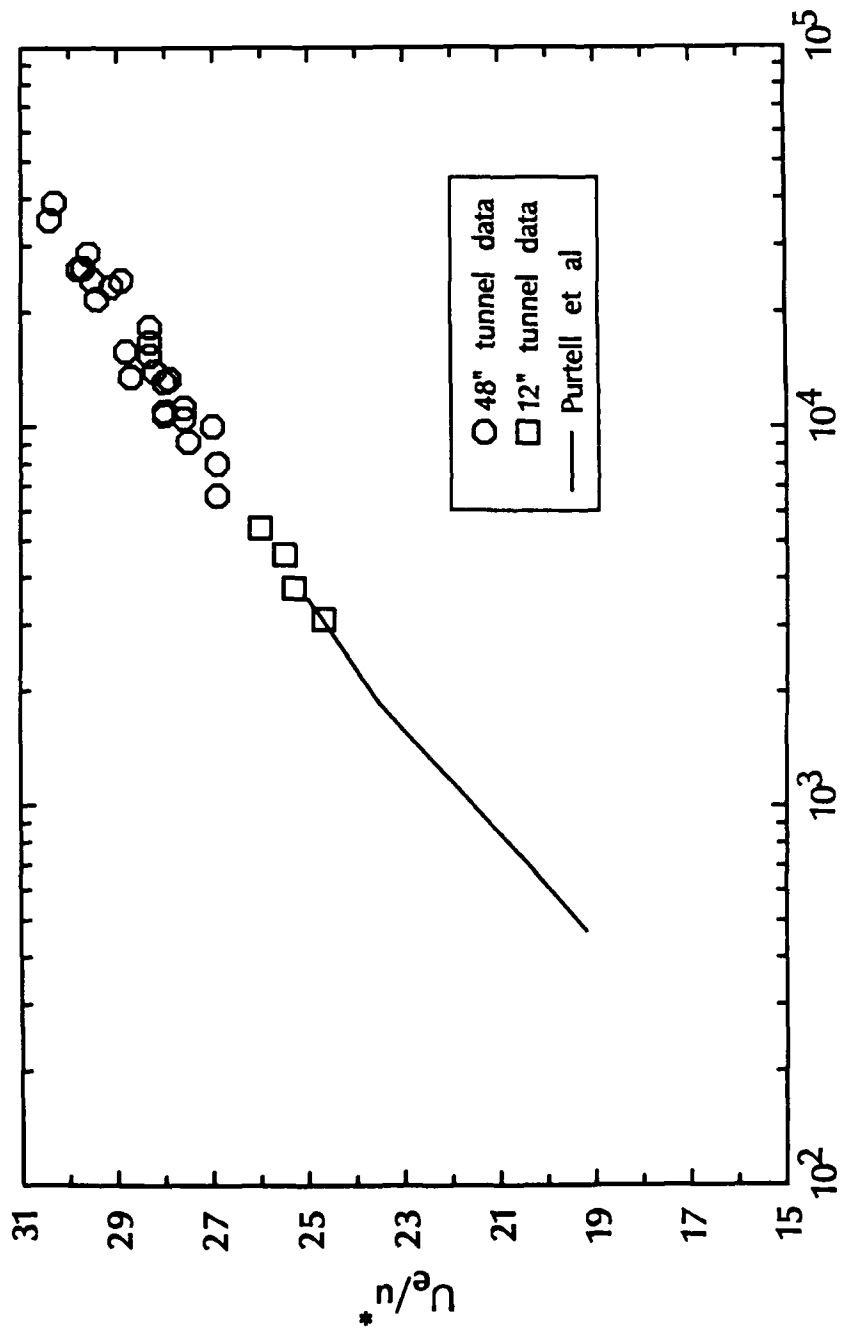

Figure 5. Variation of U_e/u^* with Re_θ Including Data from Purtell et al (1981) and 12-Inch and 48-Inch Water Tunnel Flat Plate Data

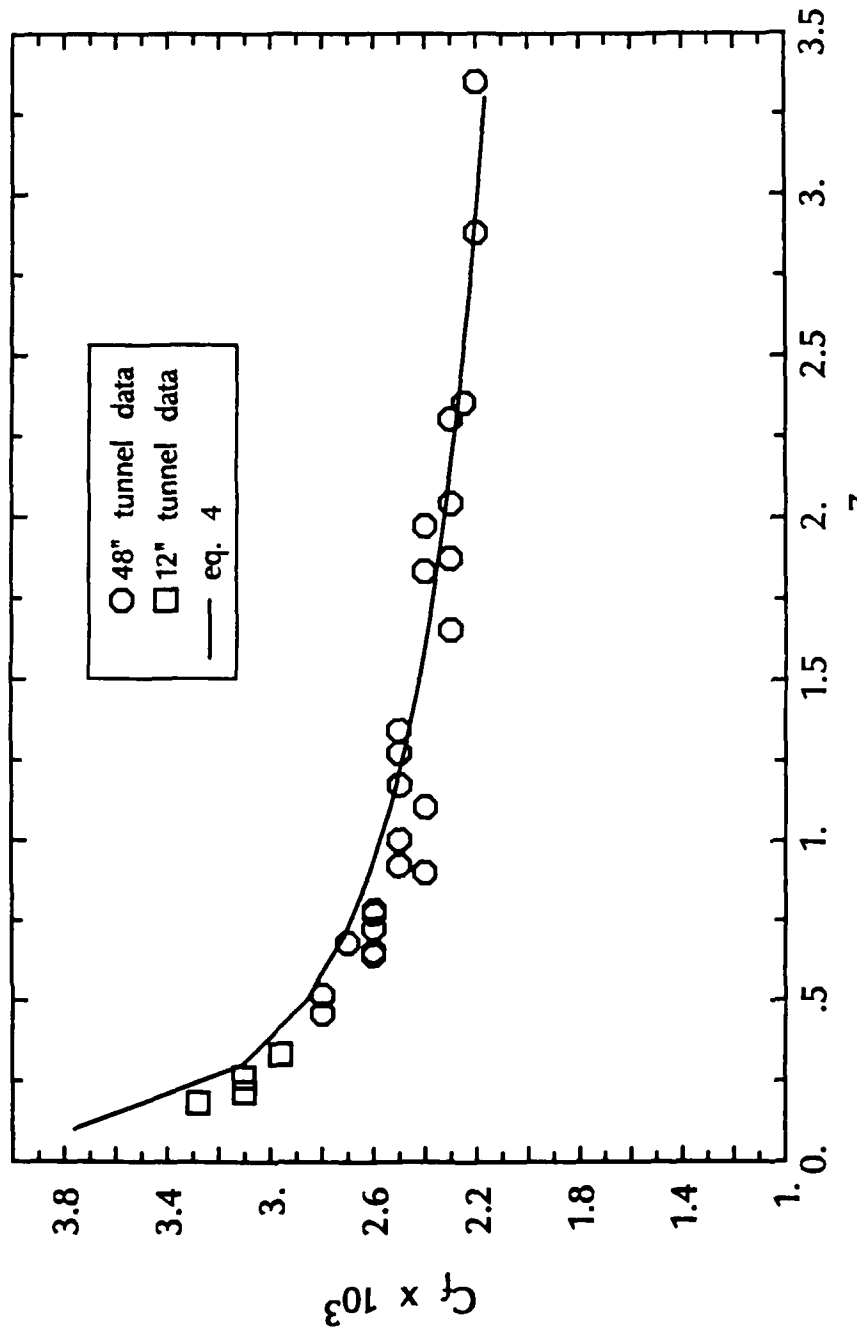

Figure 6. Large Flat Plate Skin Friction Coefficient, C_f, Data

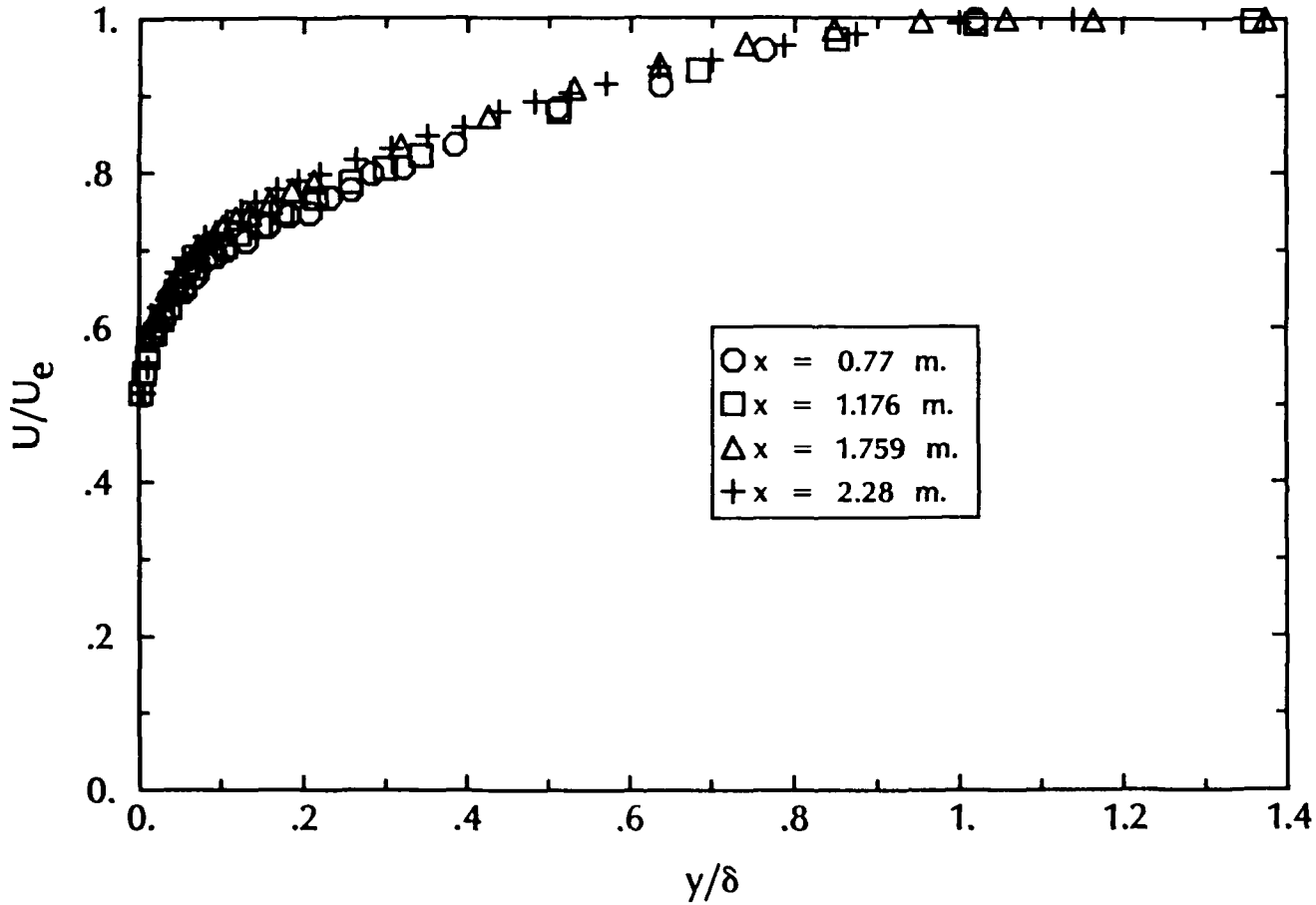

Figure 7. Mean Velocity Profiles Scaled in Outer Variables at U_e = 9.3m/s and z = 0.0m

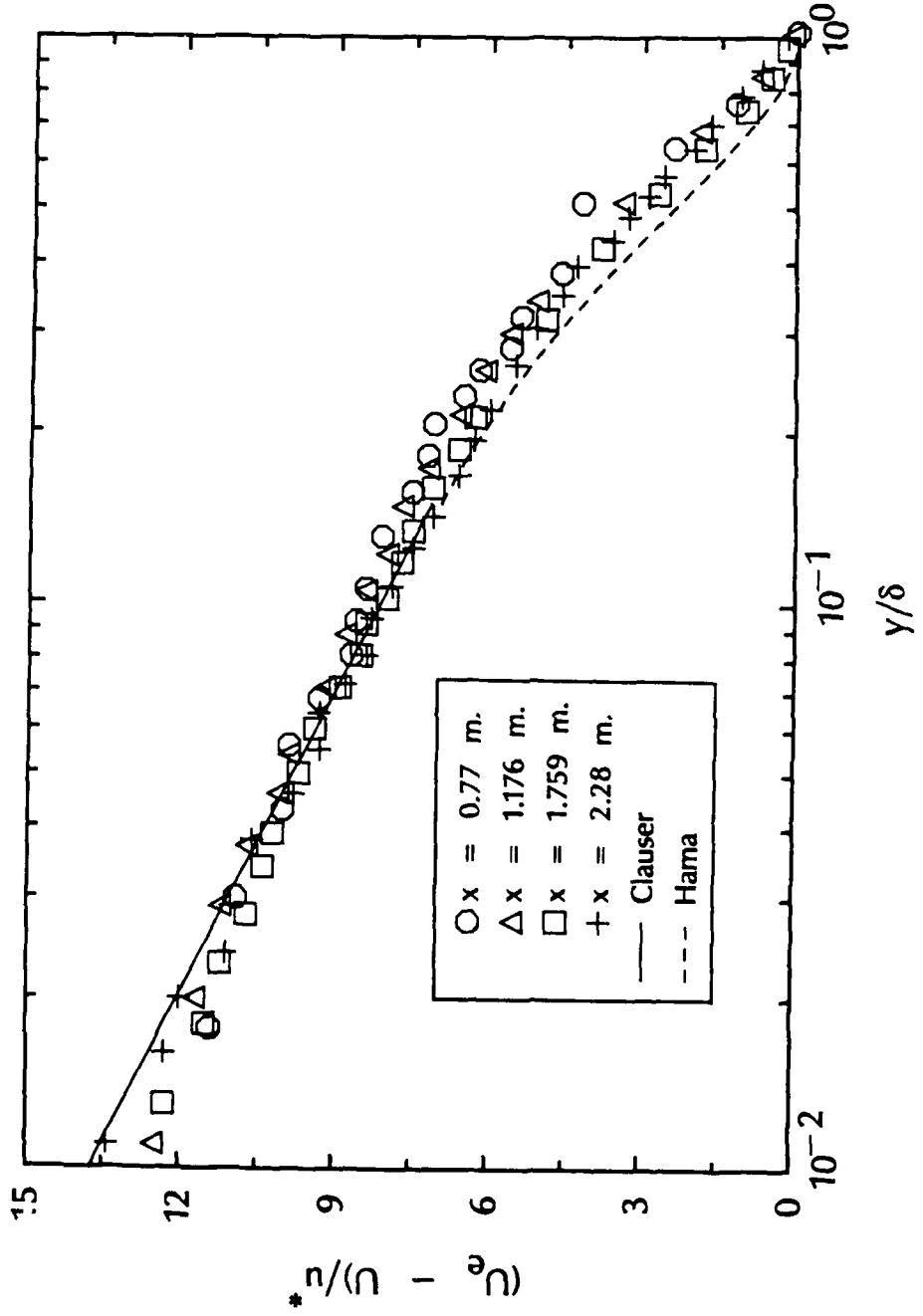

Figure 8. Large Flat Plate Velocity Defect Profiles and Equation (6) and (7)

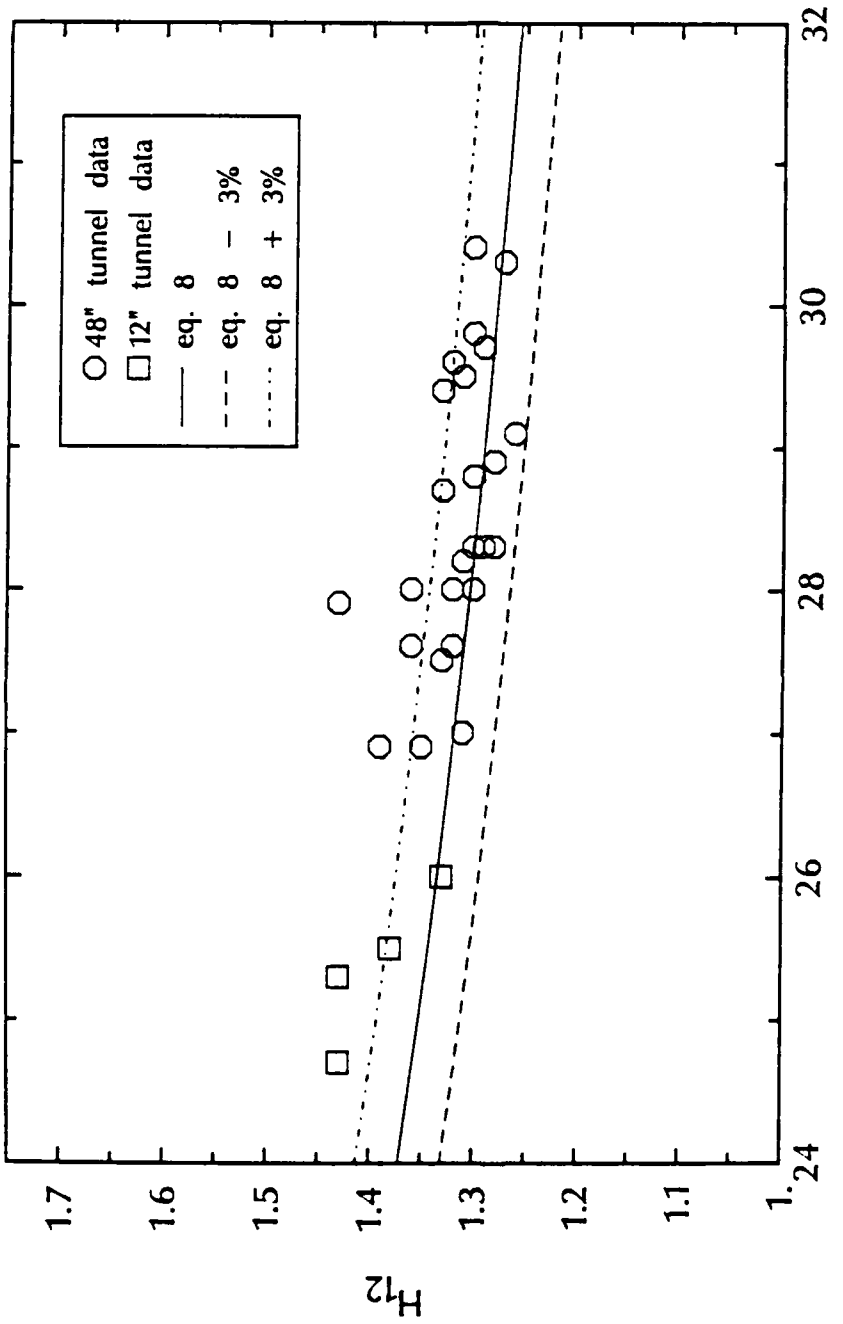

Figure 9. The Shape Factor, $H_{12} = \delta^*/\theta$, for the Large Flat Plate Data Compared with Equation (8)

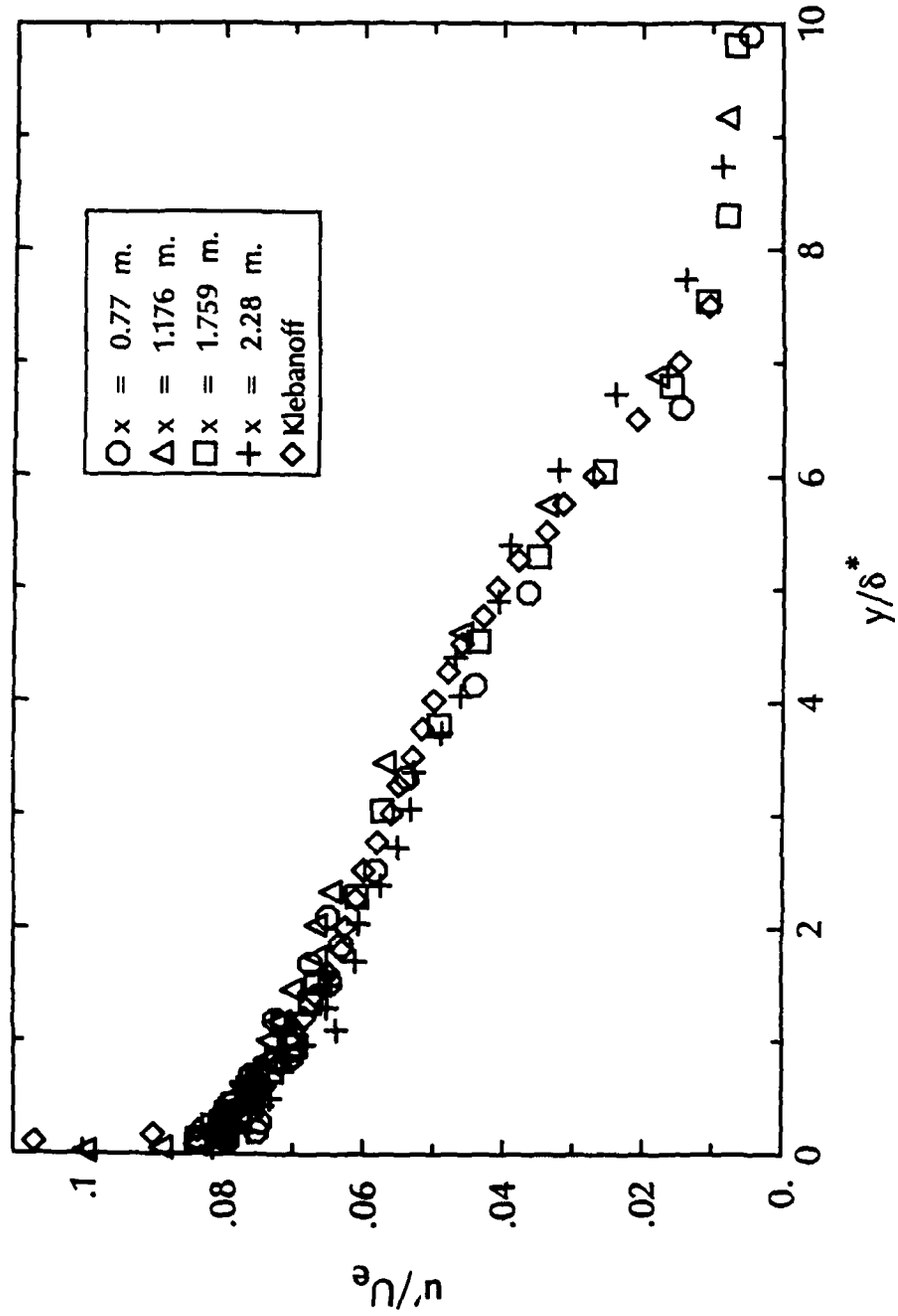

Figure 10. Streamwise RMS Fluctuation Levels Scaled in Outer Variables, U_e = 9.3m/s and z = 0.0m

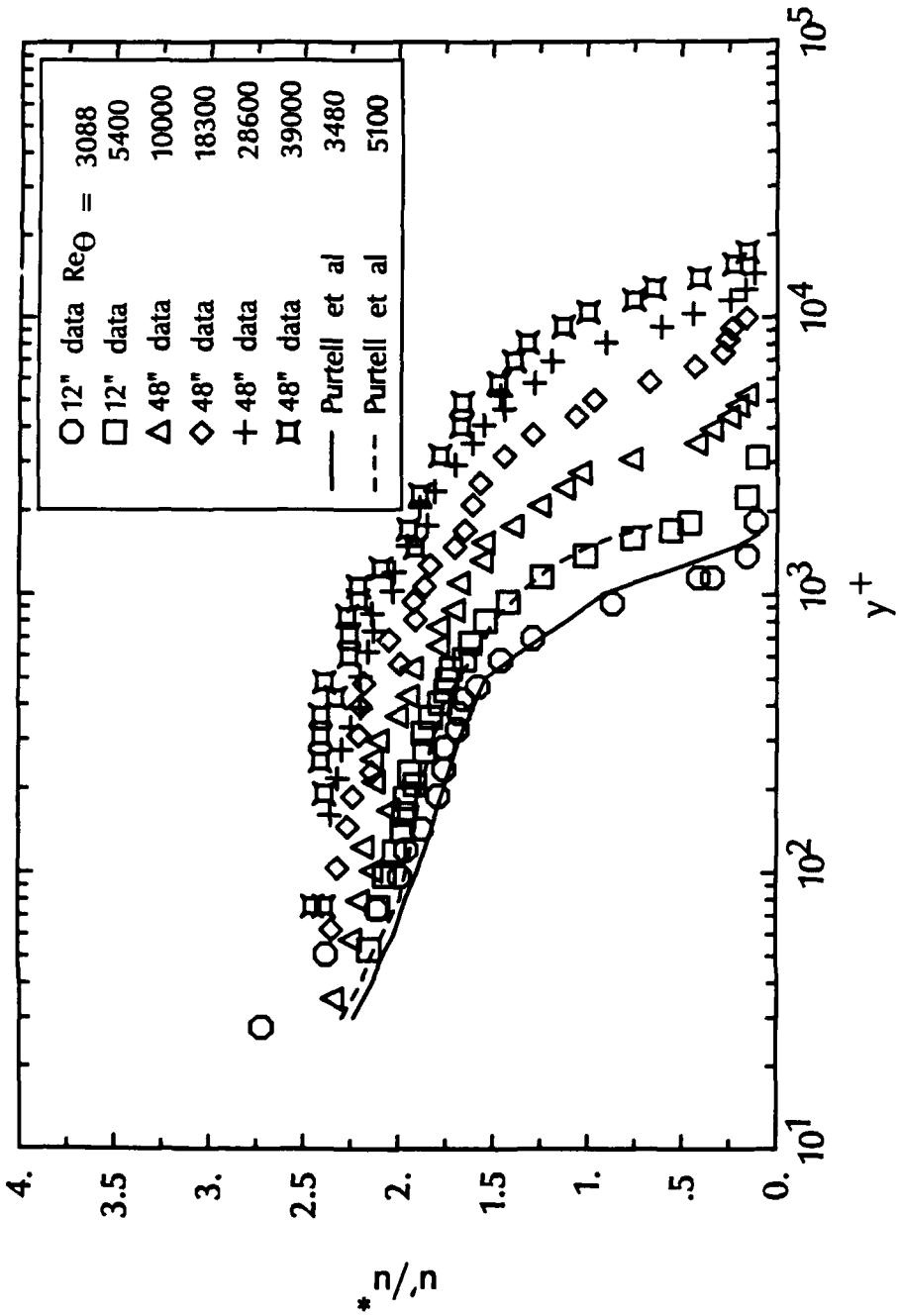

Figure 11. Streamwise RMS Fluctuation Levels Scaled in Inner Variables, U_e = 9.3m/s and z = 0.0in

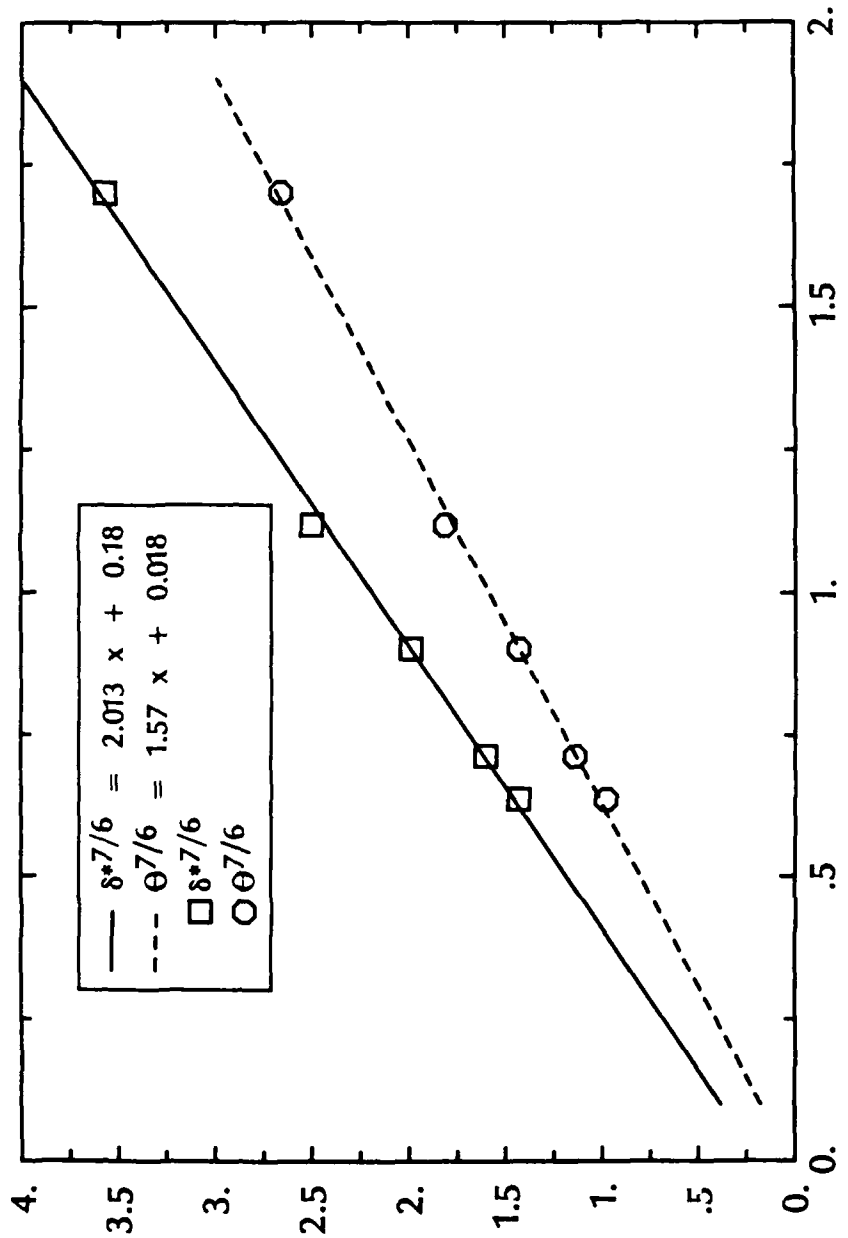

Figure 12. Estimation of the Virtual Origin Location

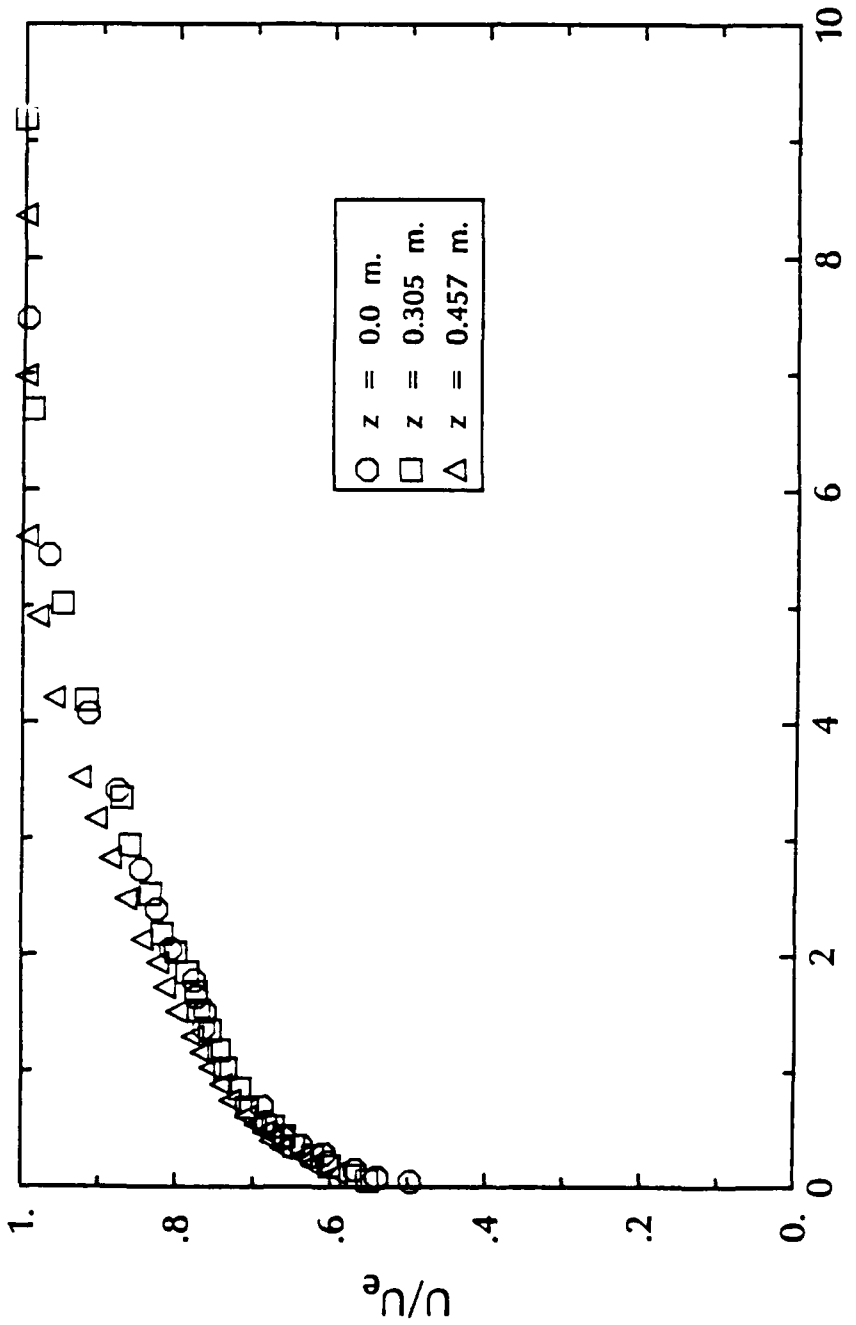

Figure 13. Mean Velocity Profiles at $z = 0.0$, 0.305, and 0.457 with $U_e = 9.3$m/s and $x_o = 0.96$m

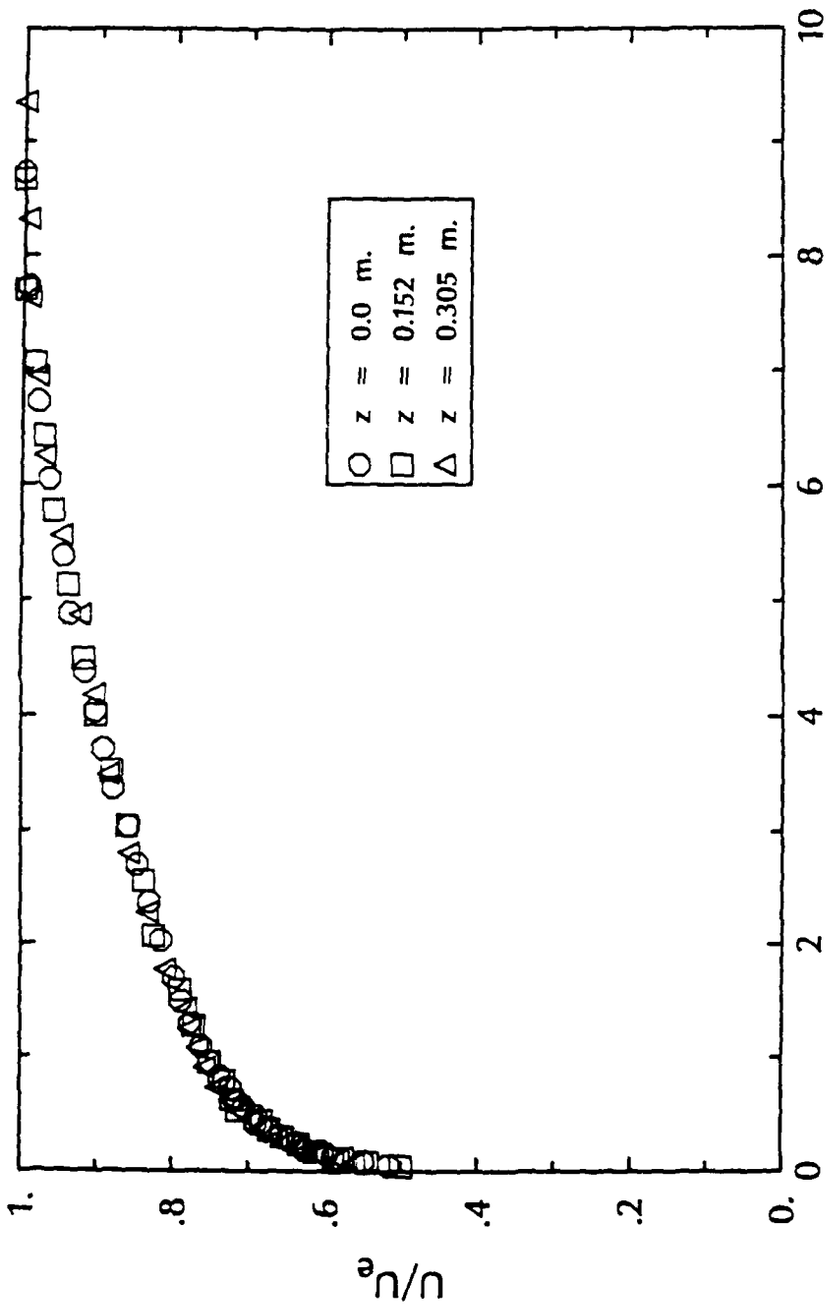

Figure 14. Mean Velocity Profiles at z = 0.0, 0.152, and 0.305m with U_e = 9.3m/s and x_o = 2.28m

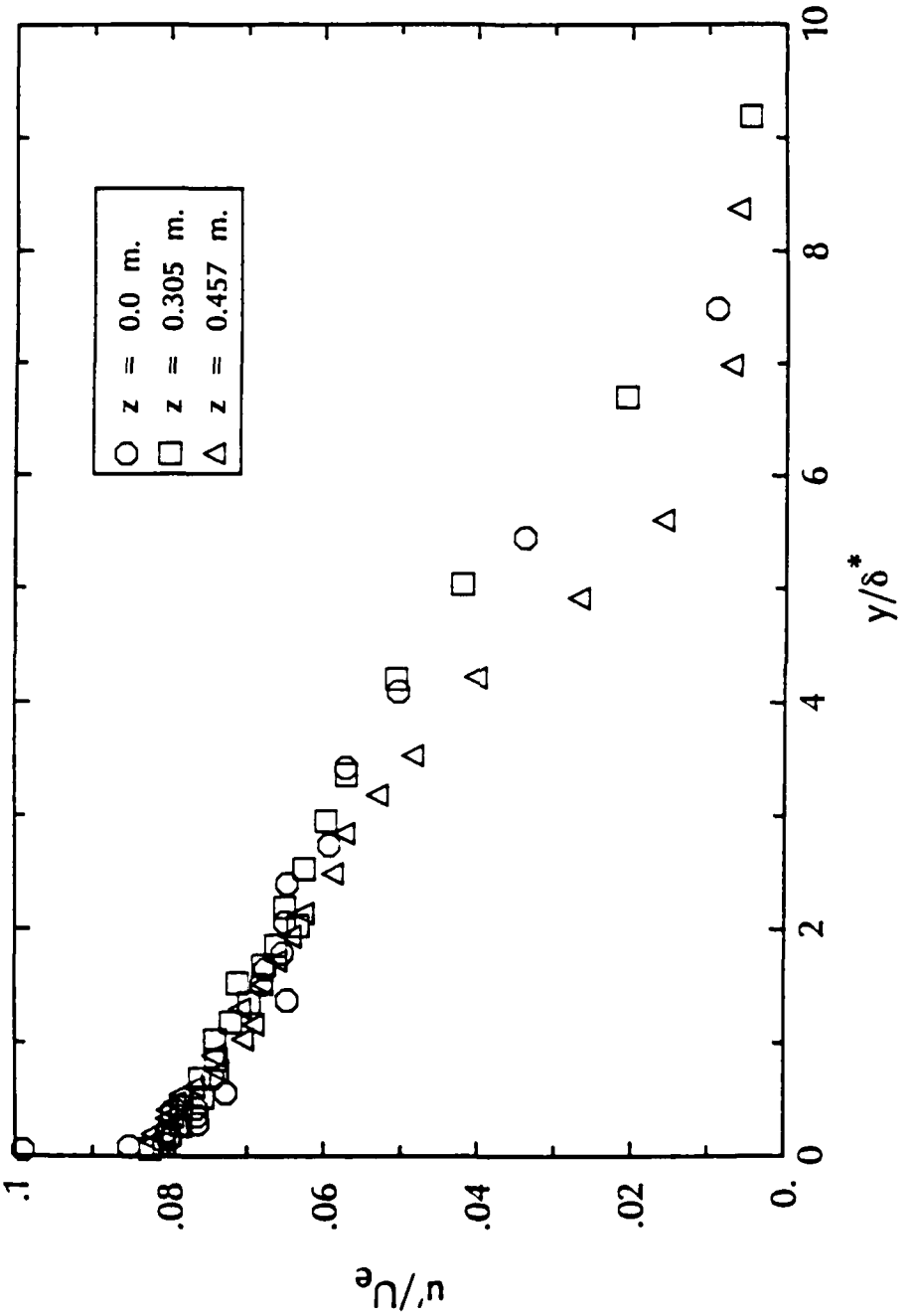

Figure 15. Streamwise RMS Fluctuation Levels at $z = 0.0$, 0.305, and 0.457m with $U_e = 9.3$m/s and $x_o = 0.96$m

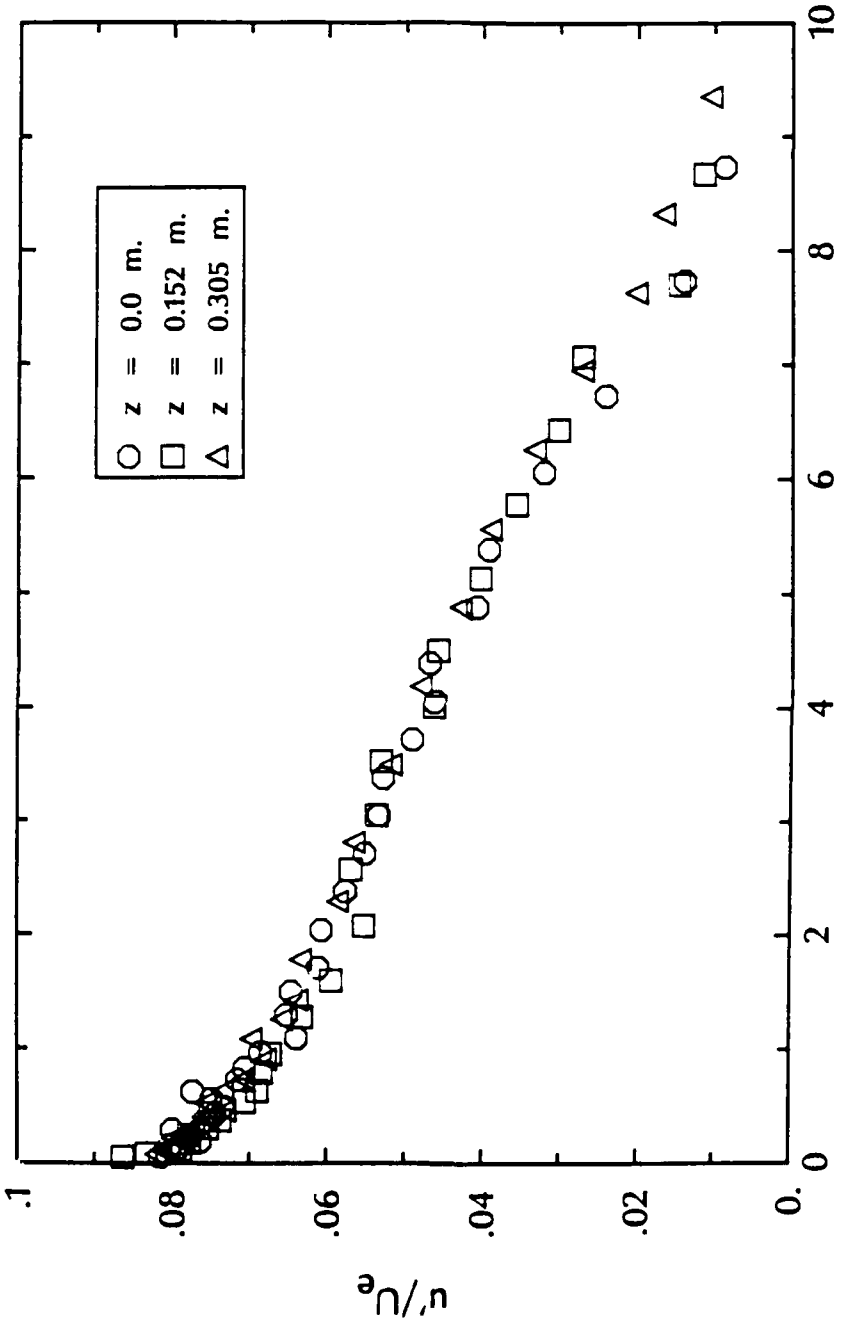

Figure 16. Streamwise RMS Fluctuation Levels at z = 0.0, 0.152, and 0.305m with U_e = 9.3m/s and x_o = 2.28m

DISTRIBUTION LIST FOR ARL UNCLASSIFIED TM 89-207 by H. L. Petrie dated 2 January 1990.

Commander Officer
Office of Naval Research
800 N. Quincy Street
Arlington, VA 22217
Attn: J. A. Fein
Code 1215
(Copy No. 1)

Commanding Officer
Office of Naval Research
Attn: R. J. Hansen
Code 1243
(Copy No. 2)

Commanding Officer
Office of Naval Research
Attn: A. D. Wood
Code ONR 12
(Copy No. 3)

Commanding Officer
Office of Naval Research
Attn: E. P. Rood
Code 1132F
(Copy No. 4)

Commanding Officer
Office of Naval Research
Attn: M. M. Reischman
Code 1132F
(Copy No. 5)

Defense Technical Information
Center (12)
Cameron Station
Alexandria, VA 22304-6145
Attn: DTIC-DDA
(Copy No. 6)

Commanding Officer
Office of Naval Technology
800 North Quincy Street
Arlington, VA 22217-5000
Attn: A. J. Faulstich
Code OCNR-23
(Copy No. 7)

Commanding Officer
Office of Naval Technology
Attn: D. C. Houser
Code ONT232
(Copy No. 8)

Commanding Officer
Naval Underwater Systems Center
Department of the Navy
Newport, RI 02841-5047
Attn: R. D. Nadolink
Code 3634
(Copy No. 9)

Commanding Officer
Naval Underwater Systems Center
Attn: R. B. Philips
Code 8214
(Copy No. 10)

Commanding Officer
Naval Underwater Systems Center
Attn: D. Goodrich
Code 3634
(Copy No. 11)

Commanding Officer
Naval Underwater Systems Center
Attn: D. Brown
Code 3634
(Copy No. 12)

Department of Ocean Engineering
Massachusetts Institute of Tech.
77 Massachusetts Ave.
Cambridge, MA 02139
Attn: P. Leehy
(Copy No. 13)

Sibley School of Mech. & Aero.
Engineering
Upson Hall
Cornell University
Ithaca, NY 14850
Attn: J. L. Lumley
(Copy No. 14)

Commanding Officer
David Taylor Research Center
Department of the Navy
Bethesda, MD 20084
Attn: J. H. McCarthy
Code 154
(Copy No. 15)

Commanding Officer
David Taylor Research Center
Attn: V. J. Monacella
Code 1504
(Copy No. 16)

David Taylor Research Center
Attn: W. Souders
Code 1543
(Copy No. 17,18,19)

Department of Aerospace Engr.
Virginia Polytechnic Institute
and State University
Blacksburg, VA 24061
Attn: Prof. R. L. Simpson
(Copy No. 20)

Department of Mechanical Engr.
Thermosciences Division
Stanford University
Stanford, CA 94305
Attn: Prof. J. P. Johnston
(Copy No. 21)

Department of Mechanical and
Ocean Engineering
University of Rhode Island
Kingston, RI 02881
Attn: Prof. F. M. White
(Copy No. 22)

Division of Engr. & Appl. Sci.
California Institute of
Technology
Pasadena, CA 91125
Attn: A. J. Acosta
(Copy No. 23)

Department of Mechanical Engr.
and Mechanics
354 Packard Laboratory, 19
Lehigh University
Bethlehem, PA 18015
Attn: Prof. D. A. Walker
(Copy No. 24)

Department of Mechanical Engr.
Purdue University
West Lafayette, IN 47907
Attn: Prof. W. Tiederman
(Copy No. 25)

Department of Aerospace and
Mechanical Engineering
Notre Dame University
Notre Dame, IN 46556-9956
Attn: Prof. Mohammad Gadelhak
(Copy No. 26)

Department of Aerospace Engr.
University of Southern California
at Los Angeles
University Park
Los Angeles, CA 90089-0192
Attn: Prof. Ron Blackwelder
(Copy No. 27)

Commanding Officer
Defense Advanced Research
Projects Agency (DARPA)
AB, Architect Building
1400 Wilson Boulevard
Arlington, VA 22209-2308
Attn: Gary Jones
(Copy No. 28)

Commanding Officer
Naval Ocean Systems Center
Department of the Navy
San Diego, CA 92152
Attn: T. Mautner
Code 6432
(Copy No. 29)

NASA Lewis Research Center
21000 Brookpark Rd.
Cleveland, OH 44135
Attn: N. Sanger
Code MS 60-5
(Copy No. 30)

NASA Langley Research Center
MS163
Hampton, VA 23665
Attn: Ben Anders
(Copy No. 31,32)

Applied Researach Laboratory
Penn State University
P.O. Box 30
State College, PA 16804
Attn: H. L. Petrie
(Copy No. 33)

Applied Research Laboratory
Attn: ARL Library
(Copy No. 33)

Applied Research Laboratory
Attn: GTWT Files
(Copy No. 34)

Unclassified
SECURITY CLASSIFICATION OF THIS PAGE

REPORT DOCUMENTATION PAGE

1a REPORT SECURITY CLASSIFICATION	1b. RESTRICTIVE MARKINGS
2a SECURITY CLASSIFICATION AUTHORITY	3 DISTRIBUTION / AVAILABILITY OF REPORT
2b DECLASSIFICATION / DOWNGRADING SCHEDULE	
4 PERFORMING ORGANIZATION REPORT NUMBER(S) TM 89-207	5 MONITORING ORGANIZATION REPORT NUMBER(S)
6a NAME OF PERFORMING ORGANIZATION Applied Research Laboratory 6b OFFICE SYMBOL (If applicable)	7a. NAME OF MONITORING ORGANIZATION
6c ADDRESS (City, State, and ZIP Code) Post Office Box 30 State College, PA 16804	7b. ADDRESS (City, State, and ZIP Code)
8a NAME OF FUNDING / SPONSORING ORGANIZATION David Taylor Research Center 8b OFFICE SYMBOL (If applicable)	9. PROCUREMENT INSTRUMENT IDENTIFICATION NUMBER N00039-88-C-0051
8c ADDRESS (City, State, and ZIP Code) Department of the Navy Bethesda, MD 20084	10 SOURCE OF FUNDING NUMBERS PROGRAM ELEMENT NO | PROJECT NO | TASK NO | WORK UNIT ACCESSION NO

11 TITLE (Include Security Classification)
Large Flat Plate Turbulent Boundary Layer Evaluation

12 PERSONAL AUTHOR(S)
H. L. Petrie, A. A. Fontaine, S. T. Sommer, T. A. Brungart

13a TYPE OF REPORT	13b TIME COVERED FROM ____ TO ____	14 DATE OF REPORT (Year, Month, Day)	15 PAGE COUNT
			33

16 SUPPLEMENTARY NOTATION

17 COSATI CODES			18 SUBJECT TERMS (Continue on reverse if necessary and identify by block number)
FIELD	GROUP	SUB-GROUP	

19 ABSTRACT (Continue on reverse if necessary and identify by block number)

The flow characteristics of a 3.1m long by 1.22m span large flat plate mounted in the test section of the ARL Penn State 48-inch diameter water tunnel have been evaluated. The turbulent boundary layer ~~(TBL)~~ over the central 50% of the span of the plate was fully developed, two dimensional and has a near zero streamwise pressure gradient. One component laser Doppler velocimeter ~~(LDV)~~ measurements were made at four freestream velocities and at nine streamwise locations on the plate. Resulting friction velocities on the plate varied from 0.175 to 0.45 m/s, approximately. Reynolds numbers, based on streamwise distance from the boundary layer virtual origin, ranged from 4.5 million to 33.5 million. Momentum thickness Reynolds numbers ranged from 6570 to 39,000. This range of momentum thickness Reynolds number is uniquely large for a laboratory flow.

20 DISTRIBUTION / AVAILABILITY OF ABSTRACT	21 ABSTRACT SECURITY CLASSIFICATION
☐ UNCLASSIFIED/UNLIMITED ☐ SAME AS RPT ☐ DTIC USERS	
22a NAME OF RESPONSIBLE INDIVIDUAL	22b TELEPHONE (Include Area Code) | 22c. OFFICE SYMBOL

DD FORM 1473, 84 MAR 83 APR edition may be used until exhausted. All other editions are obsolete.

SECURITY CLASSIFICATION OF THIS PAGE

Unclassified